Tunneling and 1/f noise currents in HgCdTe photodiodes

Y. Nemirovsky and A. Unikovsky
Kidron Microelectronics Research Center, Department of Electrical Engineering, Technion-Israel Institute of Technology, Haifa 32000, Israel

(Received 8 October 1991; accepted 12 February 1992)

The $1/f$ noise currents and the dc dark current–voltage characteristics are measured over a wide range of reverse bias voltages ($0 < V_d < -1.5$ V) and operating temperatures (30–120 K). The diodes are fabricated by ion implanting boron (n^+) on bulk p-type material with $x \approx 0.22$. Native anodic sulfide in combination with deposited ZnS is used for surface passivation. The dc dark currents of the photodiodes are modeled to extract the tunneling currents from the measured dark currents. The modeling takes into consideration diffusion, generation–recombination, and the two types of tunneling currents (trap assisted tunneling and band to band tunneling). The measurements demonstrate that the dominant mechanism that produces $1/f$ noise in HgCdTe photodiodes is tunneling, in particular trap assisted tunneling. The correlation between the $1/f$ noise currents and the dc tunneling currents is given by $\mathrm{In} = \alpha(I_t)^{\beta}(f)^{-1/2}$, where I_t is the tunneling current. The empirical factors β and α are approximately $\beta \approx 0.5$ and $\alpha \approx 1 \times 10^{-6}$ for a wide range of temperatures and reverse bias voltages, where the dominant tunneling mechanism is associated with trap assisted tunneling.

I. INTRODUCTION

$1/f$ noise, characterized by a spectrum that varies as $1/f^{\alpha}$, with α close to unity, often limits the performance of infrared focal plane arrays (IRFPAs) based on HgCdTe photodiodes coupled to silicon signal processors. Understanding the origin of $1/f$ noise in HgCdTe photodiodes is required for improving the technology of fabrication, reducing, and controlling $1/f$ noise in HgCdTe photodiode arrays.

The origin of the $1/f$ noise in HgCdTe photodiodes has been elusive as has been the origin of $1/f$ noise in electronic devices in general. In the past decade, different studies have applied several theoretical approaches and have empirically correlated $1/f$ noise in these devices with surface and bulk dark currents (Refs. 1–12 and references therein).

This study focuses on establishing the correlation between bulk tunneling and $1/f$ noise currents in HgCdTe photodiodes. The correlation between the low frequency noise current spectral density and tunneling currents of ion-implanted n^+p HgCdTe photodiodes with $x \cong 0.22$, fabricated on bulk p-type material and passivated with native anodic sulfides and evaporated ZnS, is reported. The $1/f$ noise currents and the dc dark current–voltage characteristics are measured over a wide range of reverse bias voltages and operating temperatures, in diodes with variable junction areas, to differentiate between surface and bulk effects.

We model the dc dark currents of the photodiodes to extract the tunneling currents from the measured dark currents. The modeling takes into consideration diffusion, generation–recombination and the two types of tunneling currents[13] (trap assisted tunneling and band to band tunneling). The calculated current density fits the measured current–voltage characteristics over a wide range of reverse bias voltages ($0 < V_d < -1.5$ V) and operating temperatures (30–120 K).

The present study examines the correlation between the measured $1/f$ noise currents and the modeled bulk tunneling currents in HgCdTe photodiodes. The empirical correlation and the modeling of the dc dark current components, enable us to model the $1/f$ noise current as a function of the reverse bias voltage and operating temperature.

The present results emphasize the role of bulk trap assisted tunneling currents that become dominant in photodiodes processed with a proper surface passivation technology that reduces the surface tunneling currents. The results of this study indicate the origin of the $1/f$ noise currents as well as the required material and process parameters to control and reduce the $1/f$ noise currents in focal plane arrays based on HgCdTe photodiodes.

II. TECHNOLOGY OF MATERIAL AND PHOTODIODE PROCESSING

The measurements and modeling presented in this study characterize front-illuminated, ion-implanted n^+ on bulk p-HgCdTe photodiodes with $x = 0.22$, operating near 77 K, used for hybrid focal plane arrays in the 8–12 μm spectral region. The major features of the technology of device processing and the photodiodes are as follows.

(i) The starting material is undoped crystals in which p-type conductivity is obtained with Hg vacancies.[14]

(ii) The junctions are planar and the junction periphery is covered by a metallic guard ring that is connected to the n^+ region. To differentiate between surface and bulk effects, test structures with diodes with variable junction areas are processed and measured. Junction area varies over the range 10^{-3}–10^{-5} cm^2. Smaller area photodiodes ($A_{\mathrm{opt}} = 20 \times 40$ μm^2) characterize photodiode arrays for IRFPAs. Medium area junctions are of the order of 100×100 μm^2. However, for capacitance–voltage (C–V) profiling of the junctions large area junctions (500×500 μm^2) are used. Because of the parasitic capacitance associated

 0734-211X/92/041602-09$01.00

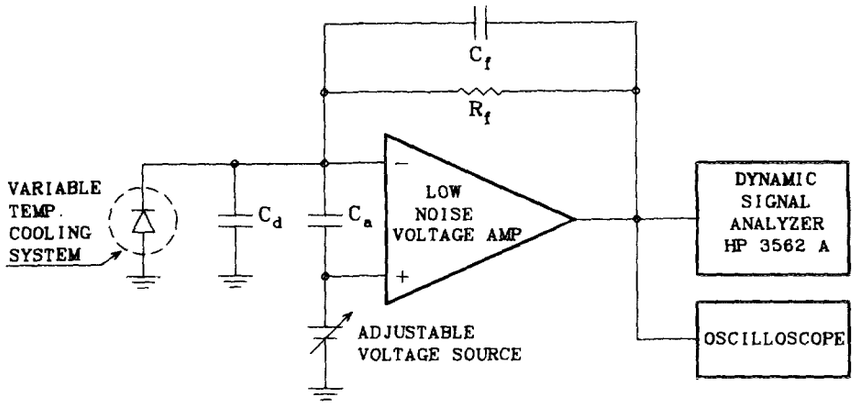

FIG. 1. Experimental setup for $1/f$ noise measurements.

with the guard ring and bonding pad, the required junction capacitance is of the order of ~ 100 pF.

(iii) n^+ shallow junctions are formed by implanting boron with a relatively low dose (3×10^{13} cm^{-2}) and low energy (~ 125 keV). The implanted junction profile is relatively complex. The electrical properties of the n^+ region are due to induced damage that extends beyond the boron implant profile. In addition, Hg atoms freed by the implant, diffuse into the p-type substrate and annihilate vacancies and decrease the doping level in the region adjacent to the junction.[15] Either an n^+p^-p graded junction or an $n^+n^-p^-p$ graded junction is formed with low p-type doping in the depletion region. Whether an n^+p^-p type of junction or an $n^+n^-p^-p$ junction is formed, is determined by the concentration of the compensating donors in the bulk p-type substrate. The complex electrical profile observed in implanted HgCdTe photodiodes is characterized with measurements of the junction capacitance as a function of the diode reverse bias voltage. With appropriate differentiation of the capacitance–voltage characteristics of large area diodes, we evaluate the impurity distribution of the junction. However, from the C–V profiles we cannot determine whether the structure is $n^+n^-p^-p$ or n^+p^-p. The complex structure of the junction and the degenerate n^+ region modify the built-in voltage (V_{bi}). The C–V characteristics exhibit a small bias region (~ 0.2 V) of nearly constant capacitance before the junction capacitance starts to decrease with applied reverse bias voltages. Hence, for modeling of the dc properties of the junctions we assume that $V_{bi} = 3$ Eg.

(iv) The diodes are passivated with native sulfides (~ 300 Å) and evaporated ZnS[16]. The interface between HgCdTe and its native sulfide in combination with ZnS has excellent electrical properties; near ideal capacitance–voltage characteristics of metal–insulator semiconductor (MIS) devices, a low fixed surface charge density, $N_{SS} \simeq -5\times10^{10}$ cm^{-2}, which imposes practically flat band conditions, a low concentration of fast interface traps ($<2\times10^{10}$ cm^{-2} eV^{-1}), and a negligible concentration of slow interface traps. With this surface passivation the contribution of surface dc dark currents and $1/f$ noise currents is small as indicated by the measurements. By measuring photodiodes with several junction areas, we can separate bulk-related currents (which increase as the junction area) and surface-related currents (which increase as the junction periphery).

(v) The junctions and photodiodes are exposed to a low temperature post implantation anneal (~ 95 °C) and temperature cycles up to 85 °C.

III. LOW FREQUENCY NOISE MEASUREMENT

The experimental setup used to measure the diode noise current spectral density is shown in Fig. 1. The photodiode noise current is amplified by a dc coupled low noise transimpedance amplifier. The input stage of the amplifier is a low noise J-FET preamplifier, to reduce the contribution of the amplifier to the total output noise.

The amplifier and setup are designed to ensure that the total noise, measured at the amplifier output is dominated by the contribution of the diode. The reverse bias current of the diode is supplied by the amplifier via the feedback resistor, connected in a negative feedback loop. The noise contribution of each component of the system is shown in Fig. 2. The noise of the feedback resistor (R_f) is modeled by thermal noise with current power spectral density of $\overline{I_n^2(R_f)} = 4kT/R_f$. The amplifier is characterized by two noise sources (a) voltage noise source in series to the input loop of the amplifier (V_{na}), and (b) current noise source in parallel to the input ports of the amplifier (I_{na}).

The voltage noise source associated with the amplifier is characterized by two components (a) shot noise with power spectral density of 2×10^{-18} V^2/Hz (or voltage density of 1.4 nV/$\sqrt{\text{Hz}}$), and (b) $1/f$ noise with power spectral density of K_f/f where $K_f = 1.6\times10^{-15}$ V^2 (or voltage spectral density of 40 nV/$\sqrt{\text{Hz}}$ at 1 Hz).

The current noise power spectral density of the measurement amplifier (I_{na}) is 3×10^{-28} A^2/Hz (or current spectral density of 1.7×10^{-14} A/$\sqrt{\text{Hz}}$ at 1 Hz).

Since the value of the feedback resistor used in the measurement amplifier is $R_f = 1$ MΩ, the current power spectral density associated with this resistor is 1.65×10^{-26}

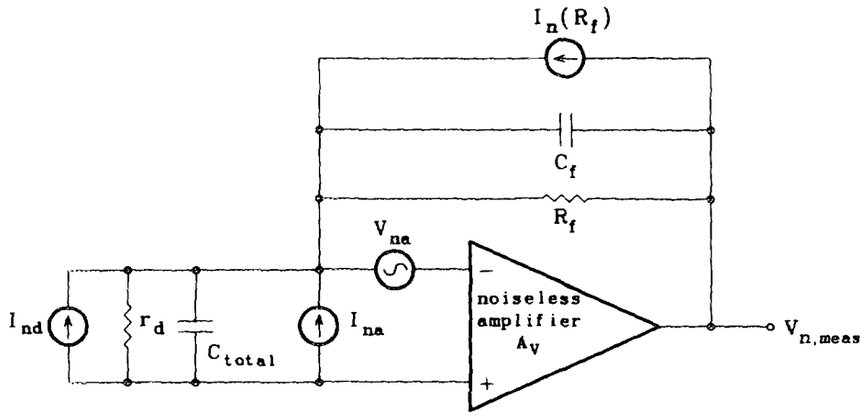

FIG. 2. The small signal equivalent circuit for the transimpedance amplifier, the diode and the bias voltage circuit. V_{na}: The root mean square (rms) noise-voltage spectral density of the amplifier, I_{na}: The rms noise current spectral density, r_d: The dynamic resistance of the diode, R_f, C_f: Feedback resistor and feedback capacitor, respectively, A_v: Open loop gain of the amplifier. $\overline{I_{nd}^2} = \overline{V_{n\,meas}^2}/R_f^2 - \overline{V_{na}^2}(1/(r_d^2) + 1/(R_f^2)) - \overline{I_{na}^2} - 4kT/(R_f)$.

A^2/Hz [or noise current spectral density of $I_n(R_f) = 1.28\times 10^{-13}$ A/$\sqrt{\text{Hz}}$]. The total noise measured at the output of the amplifier is given by

$$\overline{V_{n\ meas}^2} = R_f^2[\overline{I_{nd}^2} + \overline{I_{na}^2} + \overline{I_n^2(R_f)}] + \overline{V_{na}^2}\left(1 + \frac{R_f}{r_d}\right)^2. \tag{1}$$

The equivalent current power spectral density at the input of the amplifier is

$$\overline{I_{n\ eq}^2} = \overline{I_{nd}^2} + \overline{I_{na}^2} + \overline{I_n^2(R_f)} + \overline{V_{na}^2}\left(\frac{1}{R_f} + \frac{1}{r_d}\right)^2. \tag{2}$$

It is obvious that to get proper measurement results, the component of the measured diode's current power spectral density ($\overline{I_{nd}^2}$) should be larger than the sum of the other components.

IV. dc CHARACTERISTICS OF HgCdTe PHOTODIODES

This article focuses on the study, characterization, and modeling of "off-the-shelf" type of photodiodes obtained with the technology described in Sec. II. Figures 3 and 4 exhibit the current–voltage and dynamic resistance–voltage characteristics of a typical HgCdTe photodiode. Figure 5 exhibits the degree and quality of modeling that can be obtained with the highly simplified calculations described in the Appendix for these data that is typical of ion implanted long-wavelength infrared (LWIR) photodiodes fabricated on vacancy doped bulk p-type material with the processing technology described in Sec. II.

Figure 3 shows the $I(V)$ characteristics with diode operating temperature as a parameter, in a linear as well as a logarithmic scale for the current. The reverse characteristics extend to relatively high reverse bias voltage (~ -0.6 V) before breakdown due to the fact that the surface is practically at flat band and the fact that n^+p^-p graded junctions are formed, with low p-type doping near the n^+ region. The breakdown currents shift to slightly lower voltages as temperature is reduced, indicating that at high reverse bias voltages (> -1 V) the dominant dark current mechanism is band-to-band tunneling [see Fig. 3(a)].

At a wide range of reverse bias voltages and for temperatures below 90 K, the dark current is dominated by trap assisted tunneling, as indicated by the voltage and temper-

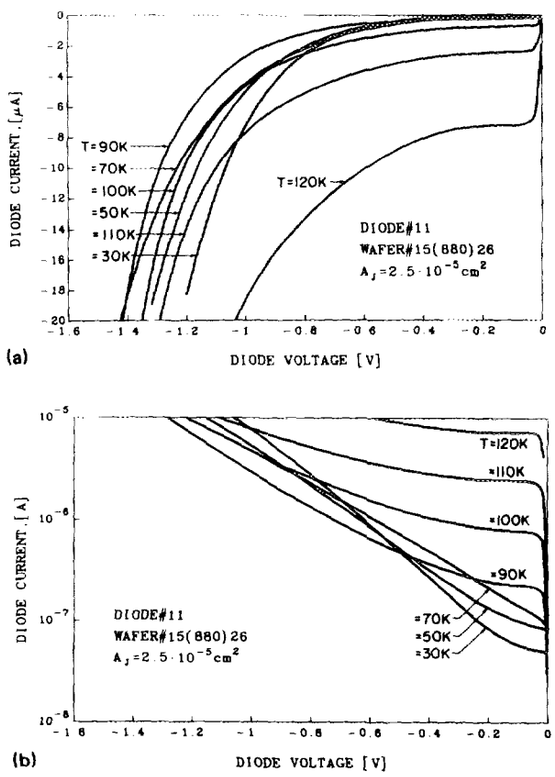

FIG. 3. Measured current–voltage characteristics of HgCdTe photodiodes with $x = 0.224$ with diode temperature as a parameter. The junction area is $A_J = 2.5\times 10^{-5}$ cm^2 and the optical area is $A_{opt} = 20\times 40(\mu\text{m})^2$. (a) Current in a linear scale and (b) current in a logarithmic scale.

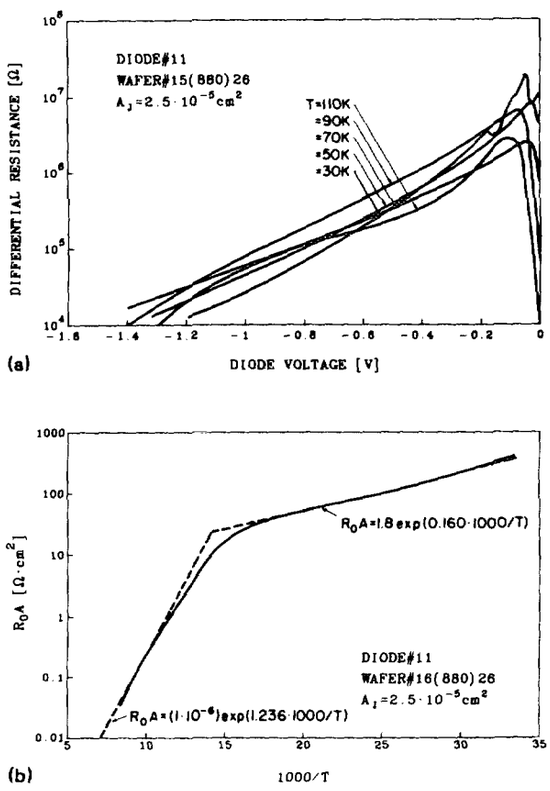

FIG. 4. (a) Dynamic differential resistance–voltage characteristics of the photodiode of Fig. 3 with diode temperature as a parameter. (b) The dependence of the measured diode zero-bias resistance area (R_0A) product on temperature.

ature dependence, exhibited in a logarithmic scale in Fig. 3(b). Above 90 K, thermal processes become dominant as indicated by the fast increase of dark current with temperature, which does not exhibit an exponential dependence on voltage.

The dark current mechanisms are also exhibited by the behavior of the dynamic differential resistance as a function of diode reverse bias voltage and operating temperature, as shown in Fig. 4(a). Below 80 K, and over a span of 1 V, the dynamic resistance exhibits an exponential dependence upon reverse bias voltage, corresponding to the $I(V)$ characteristics. In addition, the $R(V)$ characteristics exhibit only a slight dependence upon temperature between 30 to 80 K. The maximum dynamic resistance obtained at low reverse bias voltages, increases only slightly as temperature is reduced. The maximum value corresponds to the zero bias impedance obtained at $\sim$30 K indicating that the same mechanism limits the maximum dynamic resistance at 60–80 K and the R_0 at lower temperatures.

The physical mechanisms that dominate the dark properties are also exhibited by the dependence of the (R_0A) product upon reciprocal temperature, as shown in Fig. 4(b). Following DeWames,[4] the (R_0A) product is fitted with an Arrhenius plot, i.e., $(R_0A)=C\exp(E_a/kT)$. At 77 K and at higher temperatures, the dominant dark current mechanism is diffusion and $E_a=0.11$ eV which corresponds to the band gap (for $x=0.224$ and at 80 K, $E_g=0.12$ V). Below $\sim$55 K, the R_oA product approaches a plateau with a value that corresponds to the maximum dynamic resistance obtained at low reverse bias voltage, at higher temperatures. The activation energy is $\sim$14 meV, and it is possible that it indicates a shallow trap energy that limits trap assisted tunneling at lower temperatures. Between $\sim$55 and $\sim$77 K the (R_0A) product versus $1/T$ plot exhibits a transition region and it is difficult to assign an activation energy and to determine the limiting mechanism at this range of temperatures.

The dark currents are modeled with four distinct mechanisms: minority carrier diffusion from the bulk (diffusion current, J_{diff}), generation in the depletion region (g–r current, J_{gr}), trap assisted tunneling[13] (trap assisted tunneling current, J_{TAT}), and band-to-band tunneling (band-to-band tunneling current, J_{btb}). The current components are calculated in the Appendix.

Figure 5 exhibits the fit between measured and calculated current–voltage characteristics, using the four current components and the modeling described in the Appendix. A reasonable fit is obtained for a wide range of reverse bias voltages and temperatures. A more complicated type of modeling is beyond the scope of this article and will be discussed elsewhere.[17]

We model the dc dark currents of the photodiodes to extract the tunneling currents from the measured dark currents. The modeling takes into consideration two thermal components [diffusion, generation–recombination through Shockley–Read–Hall (SRH) traps] and two types of tunneling currents (trap assisted tunneling and band-to-band tunneling). In the next paragraph, we correlate the $1/f$ noise currents to the dc tunneling currents.

V. LOW FREQUENCY NOISE CHARACTERISTICS OF HgCdTe PHOTODIODES

In the low frequency range, HgCdTe photodiodes are characterized by considerable $1/f$ noise. The observed nonuniformities in the measured $1/f$ noise behavior along an array of photodiodes is larger than the nonuniformitites associated with the dc properties. These results suggest that only certain components of the total dark current are related to the $1/f$ noise current.[1,4]

Recent studies indicate that $1/f$ noise currents in HgCdTe photodiodes are related to bulk as well as surface tunneling currents. For optimized surface potentials and for high quality surface passivation which does not contribute surface dark currents, the $1/f$ noise current is due to bulk trap assisted tunneling currents.[1,2,6] The present study focuses on the correlation between the $1/f$ noise current and the component of the dc current that is associated with trap assisted tunneling.

Figure 6 exhibits the spectrum of the noise current of a typical photodiode for the technology described in Sec. II. In the low frequency range the diode exhibits $1/f$ noise that increases with the reverse bias voltage. Photodiodes coupled to silicon signal processors are operated in low reverse bias voltages where the dynamic resistance achieves

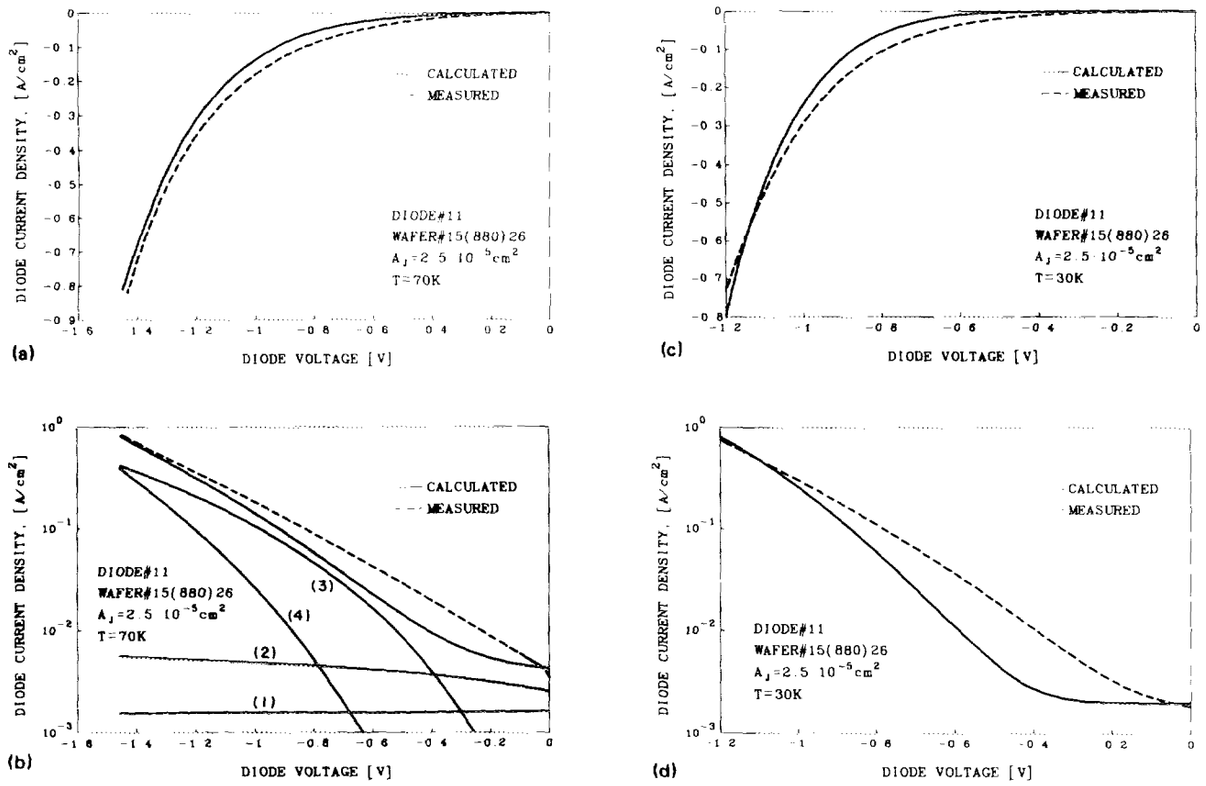

FIG. 5. Measured (dashed curve) and calculated (solid curve) current–voltage characteristics of the diode of Fig. 3. The parameters for modeling are doping level: $N_A = 1\times10^{15}$ cm^{-3} at 70 K and $N_A = 9\times10^{14}$ cm^{-3} at 30 K; trap density: $N_t = 1\times10^{14}$ cm^{-3}; capture rate: $C_p = 10^{-4}$ cm^3/s; trap energy level: $E_t = 0.7\,E_F$ (i.e., ~40 meV at 70 K and ~12 meV at 30 K). SRH lifetime at the depletion region ≃ 100 ns, and SRH lifetime at the neutral p-type region ≃ 10 ns. (a) The current is in a linear scale $T = 70$ K; (b) the current is in a logarithmic scale. $T = 70$ K; (c) the current is in a linear scale. $T = 30$ K; (d) the current is in a logarithmic scale. $T = 30$ K. The current components, including (1) diffusion current, (2) generation–recombination current, (3) trap assisted tunneling current and (4) band-to-band tunneling current, are also plotted.

higher values. Even for $V_d = -50$ meV, the noise power closely follows a $1/f$ slope.

The amplitude and the "corner frequency" where the noise $1/f$ noise becomes equal to the shot noise level of the photodiodes, increase with increasing reverse bias voltages. For photodiodes operating at reverse bias voltage, the shot noise level is given by $I_n = [2q(I_\lambda + I_o)]^{1/2}$ where I_λ is the photocurrent and I_0 is the saturation current. For a typical photodiode with $A_{opt} = 20\times40$ $(\mu m)^2$, the photocurrent is ~100 nA and the saturation current is ~10 nA, at 80 K. Hence, the noise base level is $I_n = 1.9\times10^{-13}$ A $\sqrt{\text{Hz}}$ and typical corner frequencies extend beyond 100 Hz and with increasing reverse bias voltages into the kHz frequency region. The measurements reported in this section were performed at 77 Hz, and the $1/f$ noise current spectral density is given at 1 Hz. The results of Fig. 6 indicate that the measured values are larger than the additional contribution from the measurement set up (see Sec. III).

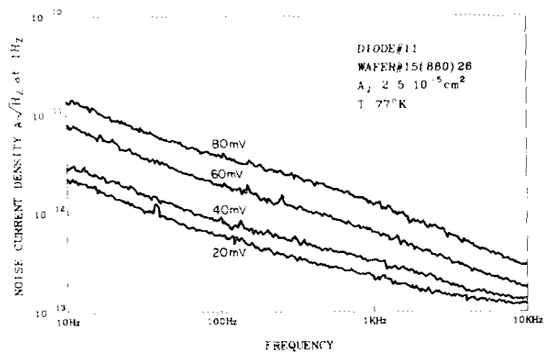

FIG. 6. Noise current spectral density of a typical photodiode (for the technology described in the article) a function of frequency, at 80 K. At 77 Hz the noise power closely follows a $1/f$ slope for reverse bias voltages. The measured noise level beyond the $1/f$ region corresponds to the shot noise level of the diode saturation current (I_0) and the photo current (I_λ), i.e. $[2q(I_\lambda + I_0)]^{1/2}$.

In order to determine the mechanism that correlates with the $1/f$ noise current, both $1/f$ noise and dark currents are measured over a wide range of reverse bias voltages and operating temperatures. By varying the diode bias, dark current and temperature, the relative contribution of each of the various current mechanisms is varied, allowing those mechanisms associated with $1/f$ noise to be isolated. Figures 7–9 exhibit the $1/f$ noise behavior of the typical photodiode that its dc characteristics are given and modeled in Sec. IV. The results suggest that only certain

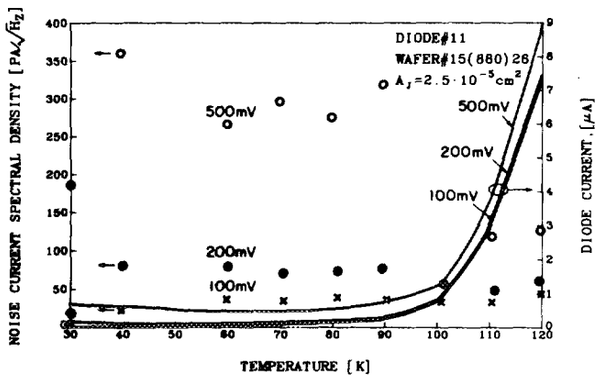

FIG. 7. Measured (dots) $1/f$ noise current spectral density at 1 Hz of the photodiode of Fig. 3 as a function of diode operating temperature at several reverse bias voltages.

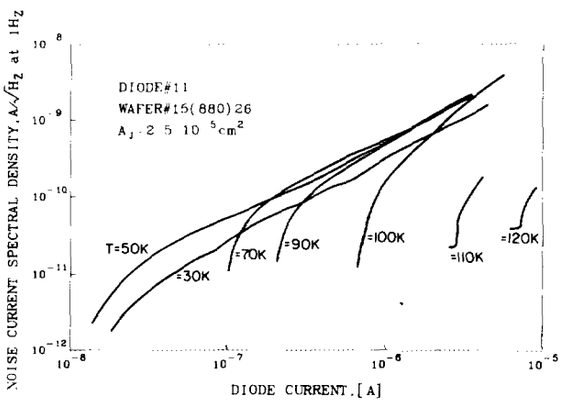

FIG. 9. Measured $1/f$ noise current spectral density at 1 Hz of the photodiode of Fig. 3 as a function of diode reverse current, with temperature as a parameter.

components of the total dark current are related to the $1/f$ noise current. From the voltage and temperature dependence of the $1/f$ noise current, the correlation with trap assisted tunneling current is established.

The temperature dependence of the dark current and $1/f$ noise current, at several reverse bias voltages, is shown in Fig. 7. The thermal generation mechanisms (diffusion, generation in the depletion region) increase with temperature. In contrast, the $1/f$ noise current is practically independent of operating temperatures indicating that a thermal generation mechanism is not related to $1/f$ noise.

The bias voltage dependence of the $1/f$ noise current is shown in Fig. 8. At higher temperatures (>80 K) and lower reverse bias voltages ($V_d < -0.3$ V), the bias dependence of the $1/f$ noise current is different from the bias dependence of the dark currents. At higher reverse bias voltages and at lower temperatures (30 K), the $1/f$ noise is found to vary with reverse bias in the same manner as the dark current, namely increases exponentially with bias.

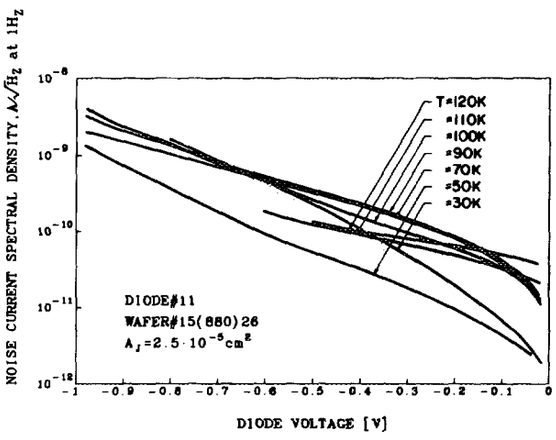

FIG. 8. Measured $1/f$ noise current spectral density at 1 Hz of the photodiode of Fig. 3 as a function of diode reverse voltage, with temperature as a parameter.

Figure 9 exhibits the measured $1/f$ noise current as a function of diode current, with temperature as a parameter. The results clearly indicate that the $1/f$ noise current is not simply related to the total current in the diode, but rather correlates with one of the mechanisms that generate the current. At lower currents the noise current increases significantly while the total current is nearly constant. Only at higher currents, the $1/f$ noise current increases with the total current. As temperature is reduced and the thermal generation mechanisms (diffusion, g–r) are reduced, the correspondence between $1/f$ noise current and diode total current is obtained at lower currents.

The correlation between the $1/f$ noise currents and the dc tunneling currents, is shown in Figs. 10 and 11. Figure 10 shows the $1/f$ noise current plotted versus the tunneling components of the dark currents of the photodiodes of Fig. 3 at 70 and 30 K. In the measured temperature range of 30–90 K, for the p-type material and technology of fabrication reported in the present study, trap assisted tunneling contributes a dominant component over a wide range of reverse bias voltages. Only at high reverse bias voltages ($V_d > -1$ V) and high currents (larger than 10^{-6} A at 70 K and 10^{-7} A at 30 K) band-to-band tunneling contributes a significant current component.

Hence, for a wide range of reverse bias voltages and operating temperatures, the $1/f$ noise current is associated with the trap assisted tunneling current and can be empirically correlated to it with $I_n = \alpha I_{\text{tat}}^{\beta}(f)^{-0.5}$ where I_n is the measured noise current, I_{tat} is the trap assisted tunneling current obtained by modeling the measured dc current–voltage characteristics, f is the frequency and $\alpha \cong 1 \times 10^{-6}$ and $\beta \cong 0.5$ are obtained from the measurements shown in Fig. 10.

At the high reverse bias voltages where there is a significant contribution of band-to-band tunneling in addition to trap assisted tunneling, the $1/f$ noise current is associated with the two components of the tunneling current and includes band-to-band tunneling as well as trap assisted tunneling. In this range (see Fig. 10), a change of slope is

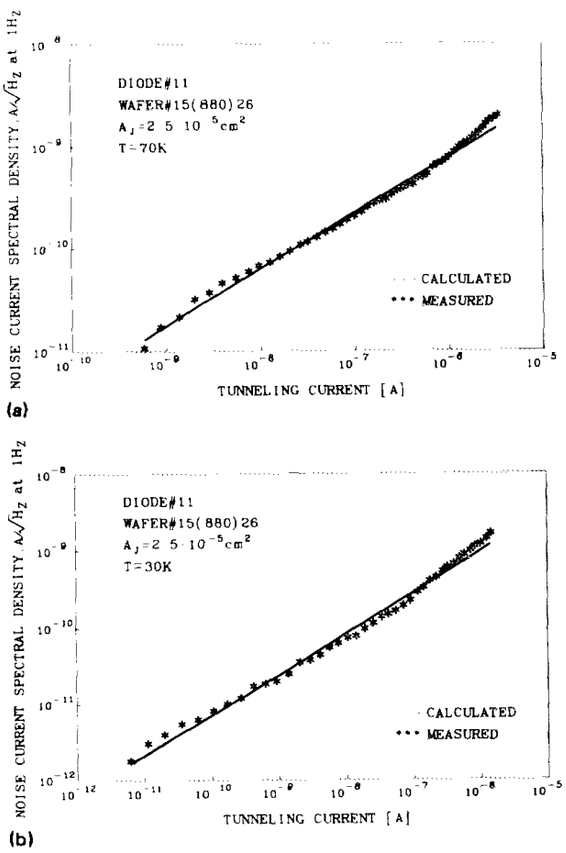

FIG. 10. Measured (dots) and calculated (solid curve) $1/f$ noise current spectral density at 1 Hz of the photodiode of Fig. 3 as a function of tunneling currents. The $1/f$ noise current at 1 Hz ($A/\sqrt{Hz}$) is calculated with $I_n = \alpha(I_t)^{\beta}(f)^{-1/2}$ where I_t is the calculated tunneling current and α and β are empirical factors. The tunneling currents are calculated with the parameters of Fig. 5. (a) Diode temperature is 70 K, $\alpha = 1.70\times10^{-6}$, and $\beta = 0.55$. (b) Diode temperature is 30 K, $\alpha = 1.39\times10^{-6}$, and $\beta = 0.53$.

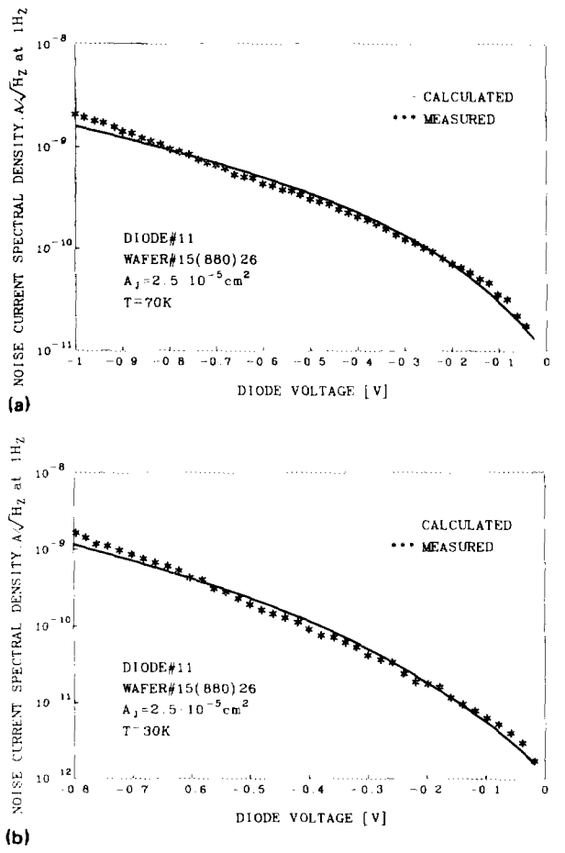

FIG. 11. Measured (dots) and calculated (solid curve) $1/f$ noise current spectral density at 1 Hz of the photodiode of Fig. 3 as a function of diode reverse voltage. The parameters for the calculations are given in Figs. 5 and 10. (a) Diode temperature is 70 K. (b) Diode temperature is 30 K.

observed and the fit is obtained with $\alpha \cong 1\times10^{-4}$ and $\beta = 0.9$.

With the empirical correlation between the dc tunneling currents and the $1/f$ noise current, we can model the noise current and calculate I_n as a function of reverse bias voltage. The calculated noise current–voltage characteristics fit the measured data in a wide range of reverse bias voltages and operating temperatures, as shown in Fig. 11. The calculations shown in Fig. 11 are based on $\alpha \cong 1\times10^{-6}$ and $\beta \cong 0.5$. The modeling fits the measured data at the low reverse bias voltages that correspond to the operating bias of HgCdTe photodiodes in IRFPAs. The fit at high reverse bias voltage can be improved by including an additional set of $\alpha \simeq 1\times10^{-4}$ and $\beta \simeq 0.9$ at this region.

VI. SUMMARY

The present study addresses the following goals.

Determination of the physical dark current mechanism that correlates with $1/f$ noise currents in HgCdTe photodiodes.

Modeling the dc and $1/f$ noise current–voltage characteristics of HgCdTe photodiodes at the operating temperatures and reverse bias voltage range that are relevant for IRFPAs.

Optimization of material requirements, design, and processing of the devices to reduce the $1/f$ noise current.

The results of recent studies indicate that the noise currents in HgCdTe photodiodes are related to bulk as well as surface tunneling currents. For optimized surface potentials and surface passivation, the $1/f$ noise current at low and medium reverse bias voltages at operating temperature ($\sim$80 K) correlates with bulk trap assisted tunneling currents (the same mechanism that limits the RA of the junction at low temperatures, i.e., below $\sim$50 K).[1,2,6,13]

The present study establishes the correlation between $1/f$ noise currents and bulk trap assisted tunneling currents by measuring the $1/f$ noise currents and dc dark current–voltages characteristics over a wide range of reverse bias voltages and operating temperatures.

We model the dc dark currents of the photodiodes to extract the tunneling currents from the measured dark currents. The empirical correlation between $1/f$ noise currents and bulk tunneling currents enables us to model the

$1/f$ noise current as a function of the reverse bias voltage and operating temperature.

The modeling takes into consideration two thermal current components (diffusion, generation–recombination through SRH traps) and two types of tunneling currents (trap assisted tunneling and band-to-band tunneling).[13] Based on the methodology presented in this article, the fit between calculated and measured characteristics can be improved by employing a more complicated type of modeling.[17]

The experimental data indicate that the $1/f$ noise current can be empirically correlated with the dc tunneling currents. The noise current is modeled using the expression

$$I_n = \alpha (I_t)^{\beta} (f)^{-0.5},$$

where I_n is the noise current spectral density ($A/\sqrt{Hz}$), I_t is the tunneling current, f is the frequency, β is a coefficient in the range of 0.5–1, depending on the type of tunneling that dominates the dark current and α is a factor with dimensions related to the particular tunneling mechanism.

For the starting material (undoped bulk p-type HgCdTe with $x \cong 0.22$) and technology of fabrication (ion implanted junctions passivated with sulfides) described in this article, trap assisted tunneling contributes a significant dark current component over a wide range of operating temperatures and reverse bias voltages. For this type of tunneling $\beta \cong 0.5$ and $\alpha \cong 1 \times 10^{-6} \sqrt{A}$. With an increasing contribution of the band-to-band tunneling current, β increases towards 1, and α increases correspondingly towards 1×10^{-3}.

The physical picture that emerges is that traps with long time constants, either in the bulk or at the surface, are responsible for the long time memory and correlation that eventually behave like $1/f$ noise. In the case of traps with long time constants, the major mechanism associated with trapping–detrapping is tunneling. Hence, there is a strong correlation between dc tunneling currents and $1/f$ noise currents. A rigorous theoretical approach based on quantum physics is required to establish this physical picture.

The data presented in this article characterize photodiodes with junction area in the range of 2.5×10^{-5} cm^{-2}–1.3×10^{-3} cm^{-2}. The fact that the same type of modeling describes the dc as well as the $1/f$ noise behavior of these diodes, indicates that bulk rather than surface effects dominate the dark current mechanisms. However, to characterize and differentiate between the surface and bulk contribution, gate controlled devices as described in Ref. 1, should be further studied.

In conclusion, high quality surface passivation with a low density of fixed, fast and slow traps is required in order to reduce the contribution of the surface to $1/f$ noise currents. The major material parameter that determines the bulk $1/f$ noise currents is the density and location of bulk traps. It is quite possible that the formation of the junction by ion implantation introduces additional bulk traps at the depletion region and hence we speculate that diffused junctions and heterojunctions obtained by epitaxial growth should exhibit less $1/f$ noise currents. It is expected that with the advent of liquid phase epitaxy and metalorganic-chemical vapor deposition, by growing the heterojunctions and the passivating layers, higher quality HgCdTe substrates, junctions, and passivation technologies will be obtained consistently and will yield IRFPAs with reduced $1/f$ noise currents.

ACKNOWLEDGMENTS

The research was supported by Technion V. P. R. Fund, Elron-Elbit Electronics Research Fund. The research was performed at the Etia and Miguel Meilechson Laboratory for advanced integrated circuit technology.

APPENDIX: DARK CURRENT MECHANISMS IN HgCdTe PHOTODIODES

1. Diffusion

The diffusion current density (J_{diff}) is given by

$$J_{diff} = \left(\frac{qn_i^2}{p_0}\right)\left(\frac{kT\mu_n}{q\tau_n}\right)^{1/2}(e^{qV_d/kT} - 1), \tag{A1}$$

where n_i is the intrinsic carrier concentration, p_0 the hole concentration taken to be equal to the net dopant concentration μ_n, τ_n the bulk minority carrier mobility and life time.

2. Generation in the depletion region

The generation current density in the depletion region J_{g-r} is given by

$$J_{g-r} = q\left(\frac{n_i}{2\tau_0}\right)X_{dep}, \tag{A2}$$

where τ_0 is the SRH life time in the depletion layer and X_{dep} is the depletion region width. For a simplified step junction

$$X_{dep} = \left(\frac{2\epsilon_0\epsilon_s V_t}{qN_A}\right)^{1/2}, \tag{A3}$$

where $V_t = V_{bi} + V_d$ is the total junction potential and is the sum of the built-in potential V_{bi} and the diode reverse voltage V_d. According to Sec. II, a graded junction approximation is more appropriate. Since the grading factor is not obtained from measured data, we have used the simplified step junction where N_A is the effective doping in the depletion region. We assume that $V_{bi} \cong 3$ Eg as discussed in Sec. II.

3. Trap assisted tunneling (Refs. 13 and 18)

Trap assisted tunneling can occur via (1) a thermal transition to SRH center in the band gap located at an energy E_t from the valence band, with rate C_pP_1 and (2) tunnel transitions with rate w_vN_v followed by (3) tunnel transitions to the conduction band with rate w_cN_c. C_p is the hole capture coefficient, $P_1 = N_1 \exp[-E_t/kT]$, w_vN_v and w_CN_C are the tunneling rates from the valence band to the trap and from the trap to the conduction band, respectively.

The trap assisted tunneling current density is given by

$$J_{\text{tat}} = qN_t\left(\frac{1}{C_pP_1 + w_vN_v} + \frac{1}{w_cN_c}\right)^{-1} X_{\text{dep}}. \quad \text{(A4)}$$

For the limiting case $w_cN_c < C_pP_1$ and $w_vN_v \cong w_cN_c$,

$$J_{\text{tat}} \simeq qN_t(w_cN_c)X_{\text{dep}}. \quad \text{(A5)}$$

Following Kinch,[18] the tunneling rate w_cN_c is given by

$$w_cN_c = \frac{6\times 10^5 E}{(Eg - Et)} \times \exp\left(\frac{-1.7\times 10^7 Eg^{1/2}(Eg - Et)^{3/2}}{E}\right), \quad \text{(A6)}$$

where the electric field E is $E = qN_AX_{\text{dep}}/(\epsilon_0\epsilon_S)$ (V/cm) and E_g and E_t are in volts.

We assume that there are several traps and that the dominant trap energy in the trap assisted tunneling process is temperature dependent. For modeling, we can optimize E_t as a parameter at each temperature. We can simplify the modeling by assuming that the temperature dependence approximately corresponds to the Fermi level E_F. Hence,

$$E_t = tE_F = t\left[\frac{E_g}{2} + \frac{kT}{q}\ln\left(\frac{m_n^*}{m_e^*}\right)^{3/4} - \frac{kT}{q}\ln\left(\frac{N_A}{n_i}\right)\right], \quad \text{(A7)}$$

where t is a factor. For the modeling of the diode of Fig. 3 we assume that $t = 0.7$ through the whole temperature range 30–90 K.

4. Band-to-band tunneling (Ref. 18)

The direct band-to-band tunneling current density J_{btb} is given by

$$J_{\text{btb}} = 10^{-2}N_A^{1/2}V_t^{3/2}\exp\left[\frac{-4.3\times 10^{10}Eg^2}{(N_AV_t)}\right]. \quad \text{(A8)}$$

[1] Y. Nemirovsky and D. Rosenfeld, J. Vac. Sci. Technol. A **8**, 1159 (1990).
[2] Y. Nemirovsky, D. Rosenfeld, R. Adar, and A. Korenfeld, J. Vac. Sci. Technol. A **7**, 528 (1989).
[3] A. van der Ziel, P. Fang, L. He, X. L. Wu, A. D. Van Rheenen, and P. H. Handel, J. Vac. Sci. Technol. A **7**, 550 (1989).
[4] R. E. DeWames, J. G. Pasko, E. S. Yao, A. H. B. Vanderwyck, and G. M. Williams, J. Vac. Sci. Technol. A **6**, 2655 (1988).
[5] A. van der Ziel, *Noise in Solid State Devices and Circuits* (Wiley, New York, 1985).
[6] Y. Nemirovsky, R. Adar, A. Korenfeld, and I. Kidron, J. Vac. Sci. Technol. A **4**, 1986 (1986).
[7] A. van der Ziel, P. H. Handel, X. L. Wu, and J. B. Anderson, J. Vac. Sci. Technol. A **4**, 2205 (1986).
[8] T. G. Kleinpenning, J. Vac. Sci. Technol. A **3**, 176 (1985).
[9] W. A. Radford and C. E. Jones, J. Vac. Sci. Technol. A **3**, 183 (1985).
[10] H. K. Chung, A. M. Rosenberg, and P. H. Zimmermann, J. Vac. Sci. Technol. A **3**, 89 (1985).
[11] J. Bajaj, G. M. Williams, N. H. Sheng, M. Hinnrichs, D. T. Cheung, J. P. Rose, and W. E. Tennant, J. Vac. Sci. Technol. A **3**, 192 (1985).
[12] S. P. Tobin, S. Iwasa, and T. J. Tredwell, IEEE Trans. Electron Devices **27**, 43 (1980).
[13] Y. Nemirovsky, R. Fastow, M. Meyassed, and A. Unikovsy, J. Vac. Sci. Technol. B **9**, 1829 (1991).
[14] E. Finkman and Y. Nemirovsky, J. Appl. Phys. **59**, 1205 (1986).
[15] L. O. Bubulac and W. E. Tennant, Appl. Phys. Lett. **51**, 355 (1987).
[16] Y. Nemirovsky and G. Bahir, J. Vac. Sci. Technol. A **7**, 450 (1989).
[17] A. Univosky, M. Sc. Thesis, Technion, 1992.
[18] D. K. Blanks, J. D. Beck, M. A. Kinch, and C. Colombo, J. Vac. Sci. Technol. A **6**, 2790 (1988).